INTERFACE

royalsocietypublishing.org/journal/rsif

Research

Cite this article: Li S, Wang C, Nithiarasu P. 2019 Electromechanical vibration of microtubules and its application in biosensors. *J. R. Soc. Interface* **16**: 20180826.
http://dx.doi.org/10.1098/rsif.2018.0826

Received: 4 November 2018
Accepted: 16 January 2019

Subject Category:
Life Sciences–Physics interface

Subject Areas:
biomechanics, biomaterials, nanotechnology

Keywords:
microtubules, electromechanical vibration, elastic moduli, tubulin interaction

Author for correspondence:
Chengyuan Wang
e-mail: chengyuan.wang@swansea.ac.uk

Electronic supplementary material is available online at https://doi.org/10.6084/m9.figshare.c.4381763.

THE ROYAL SOCIETY PUBLISHING

Electromechanical vibration of microtubules and its application in biosensors

Si Li, Chengyuan Wang and Perumal Nithiarasu

Zienkiewicz Centre for Computational Engineering, College of Engineering, Swansea University, Bay Campus, Fabian Way, Swansea SA1 8EN, UK

CW, 0000-0002-1001-2537

An electric field (EF) has the potential to excite the vibration of polarized microtubules (MTs) and thus enable their use as a biosensor for the biophysical properties of MTs or cells. To facilitate the development, this paper aims to capture the EF-induced vibration modes and the associated frequency for MTs. The analyses were carried out based on a molecular structural mechanics model accounting for the structural details of MTs. Transverse vibration, radial breathing vibration and axial vibration were achieved for MTs subject to a transverse or an axial EF. The frequency shift and stiffness alteration of MTs were also examined due to the possible changes of the tubulin interactions in physiological or pathological processes. The strong correlation achieved between the tubulin interaction and MT vibration excited by EF provides a new avenue to a non-contacting technique for the structural or property changes in MTs, where frequency shift is used as a biomarker. This technique can be used for individual MTs and is possible for those in cells when the cytosol damping on MT vibrations is largely reduced by the unique features of MT–cytosol interface.

1. Introduction

Microtubules (MTs) are fundamental structural elements in the cytoskeleton of eukaryotic cells. They provide mechanical support for the shape of cells, form tracks for directed subcellular transport and are part of the spindle apparatus important for cell division [1,2]. MTs are composed of heterodimer subunits of α and β tubulins which carry unbalanced negative charge [3,4]. This biophysical property of tubulin endows MTs with the ability to respond to an external electric field (EF) [5,6].

The vibration of MTs has attracted considerable attention in the last two decades [7–13]. Recently, the electromechanical vibration of MTs was excited by applying an external EF [2], showing the potential of polarized MTs as biosensors in disease diagnosis and health monitoring. It thus becomes essential to gain an in-depth understanding of the electromechanical vibration of MTs subject to an EF [2,14]. A theoretical study was first conducted to quantitatively describe the EF generated by a vibrating MT [6], which provides a means to detect the vibration of MTs. After that, an optomechanical technique [2] was proposed to probe and, more importantly, stimulate the vibration via EF on MTs modelled as a one-dimensional structure. However, MTs are actually three-dimensional discrete structures composed of charged subunits. It is thus of great interest to explore the behaviour of EF-induced vibration of MTs as three-dimensional nanostructures. In existing studies, vibration analyses were carried out for MTs first in the framework of continuum mechanics theory [10,11]. Subsequently, discrete approaches were developed to account for nanoscale MT structure and its influence on MT vibration [13]. The typical examples are the molecular dynamics (MD) simulations [15–17] and the cost-effective molecular structural mechanics (MSM) model [18].

In this paper, the MSM model [18] is again employed to simulate the vibration of MTs subject to an alternating EF generated by a dipole antenna. The vibration spectra are recorded for MTs for various possible modes. In addition, the correlation between frequency shift and the possible softening/hardening of MTs is quantified demonstrating the potential application of vibrating MTs as biosensors. In addition, a parametric study is also conducted to evaluate the damping effect of surrounding cytosol, which could be reduced by the nanoscale MT–cytosol interface. The paper is organized as follows. The simulation set-up, i.e. an MT subject to an alternating EF of dipole antenna, is illustrated in §2. The simulation results and corresponding discussions are given in §3, and the conclusions are drawn in §4.

2. Model development and vibration excitation

2.1. Molecular structural mechanics model for microtubule structure

In this work, 13–3 MTs are considered as a typical example, which have 13 proto-filaments and helix start $S = 3$ [19] as shown in figure 1*a*. The details of the helix nanostructure were characterized by an MSM model [18] in figure 1*b* where the blue balls denote α tubulins and the red balls represent β tubulins. In addition, the intra-PF $\alpha\beta$ interactions of MTs are modelled as the longitudinal elastic space beams while the inter-PF $\alpha\alpha$ ($\beta\beta$) interaction are treated as the helical space beams. Following previous studies [16,18,20], the small difference in $\alpha\alpha$ and $\beta\beta$ interactions is neglected. Such a frame structure model is developed to account for the configuration details, the tubulin interaction and various deformation patterns (figure 1*c*) of 13–3 MTs at the nanoscale.

In molecular mechanics, the force field is expressed in the form of steric potential energy. The major parts of the steric potential energy of an MT structure include the bond stretching energy U_i^r, the angle bending energy U_i^φ and the dihedral angle torsional potential energy U_i^τ. The total potential energy U of an MT reads

$$U_{\text{bonds}} = \sum_{i=1,2}\left(\sum U_i^r + \sum U_i^\varphi + \sum U_i^\tau\right), \tag{2.1}$$

where i denotes the types of bonds mentioned above ($i = 1$ for the intra-PF bonds and $i = 2$ for the inter-PF bonds). The expressions for the three types of bond energy are as follows:

$$\left.\begin{aligned} U_i^r &= \tfrac{1}{2}k_i^r(\Delta r_i)^2\,, \\ U_i^\varphi &= \tfrac{1}{2}k_i^\varphi(\Delta\varphi_i)^2 \\ \text{and}\quad U_i^\tau &= \tfrac{1}{2}k_i^\tau(\Delta\Phi_i)^2, (i = 1,2). \end{aligned}\right\} \tag{2.2}$$

Here, as shown in figure 1*c*, Δr_i is the change of bond length, $\Delta\varphi_i$ is the change of in-plane bond angle, $\Delta\Phi_i$ is the change of out-of-plane angle, k_i^r is the force constant for bond stretching, k_i^φ is the force constant for bond angle bending and k_i^τ is the force constant for bond torsion. The values of these force constants can be obtained in atomistic simulations or experiments.

Also, the total potential energy of the MSM model can be written as

$$U_{\text{beams}} = \sum_{i=1,2}\left(\sum U_i^A + \sum U_i^M + \sum U_i^T\right), \tag{2.3}$$

where U_i^A is the strain energy of a beam in tension, U_i^M is the strain energy due to bending, U_i^T is the strain energy due to torsion and i specifies the quantities of beam i ($i = 1$ for longitudinal beams and $i = 2$ for lateral beams). The beam energy is calculated by using the following formulae:

$$\left.\begin{aligned} U_i^A &= \frac{1}{2}\frac{Y_iA_i}{l_i}(\Delta l_i)^2, \\ U_i^M &= \frac{1}{2}\frac{Y_iI_i}{l_i}(2\Delta\alpha_i)^2 \\ \text{and}\quad U_i^T &= \frac{1}{2}\frac{S_iJ_i}{l_i}(\Delta\beta_i)^2, (i = 1,2). \end{aligned}\right\} \tag{2.4}$$

As shown in figure 1*d*, Δl_i is the length change of the beam, $\Delta\alpha_i$ is the bending angle, $\Delta\beta_i$ is the torsion angle, $Y_i\,A_i$ is the extensional stiffness, $Y_i\,I_i$ is the bending stiffness and S_iJ_i is the torsional stiffness of the beams.

The equivalency of the MT structure and its MSM model can be established when the corresponding energies in equations (2.2) and (2.4) are equal, which leads to the following relationship between the force constants of the bonds and the stiffnesses of the space beams:

$$\frac{Y_iA_i}{l_i} = k_i^r,\ \frac{Y_iI_i}{l_i} = k_i^\varphi,\ \frac{S_iJ_i}{l_i} = k_i^\tau, (i = 1,2). \tag{2.5}$$

In this study, the values of k_i^r, k_i^φ, k_i^τ were obtained from the MD simulations in [18,21,22] and further optimized in [23], i.e. $k_1^r = 3\,\text{nN nm}^{-1}$, $k_1^\varphi = 2\,\text{nN nm}^{-1}$, $k_1^\tau = 0.04\,\text{nN nm}^{-1}$, $k_2^r = 0.14\,\text{nN nm}^{-1}$, $k_2^\varphi = 0.085\,\text{nN nm}^{-1}$, $k_2^\tau = 0.0017\,\text{nN nm}^{-1}$. Then, the values of the beam stiffnesses required in the MSM simulations of 13–3 MTs can be obtained by using equation (2.5). The MSM model was employed to perform the simulations on the electromechanical vibration of 13–3 MTs.

2.2. Excitation and damping of microtubule vibrations

The migration of individual MTs in an EF has been observed via video contrast microscopy [3]. In this process, the magnitude of the unbalanced negative charge carried by tubulins was found to be lower than the theoretical one due to the effects of the electroosmotic flow and the surrounding substances [3]. Also, this magnitude varies from one experiment to another [3,24–26]. On the other hand, the computer simulations from crystallographic data gave an identical value of -5 electron charges for the tubulin monomer isolated from environment [3,27,28]. As such, the charge carried by one monomer was set to $q = -5e$ [28] in the present work. Figure 2 shows an alternating EF generated by a Hertzian dipole in a spherical polar coordinate system characterized by the radial distance (r), polar angle (θ) and azimuthal angle (Ψ) coordinators. The mathematical description of the EF can be found in [29–31]. Herein, we have placed a 13–3 MT (1 µm in length) at a point with $\theta = 0$ and $r = 0.1$ m, and the axial direction of the MT is in either azimuthal angle direction $\hat{\Psi}$ (the unit vector) or polar angle direction $\hat{\theta}$ (figure 2). When the radial distance r of the MT is much greater than its length, the EF can be approximated as a uniform EF exhibiting harmonic time dependence. The amplitude of the EF is set to $|\boldsymbol{E}| = 20\,\text{V m}^{-1}$.

Here, figure 2 graphically illustrates a prototype design of MT-based biosensors where an alternating EF is generated by an electronic device (represented by a dipole here) and used to excite the vibration of individual MTs which are a distance away from the electronic device. The frequency shifts of MTs can then be employed as a biomarker to monitor the changes

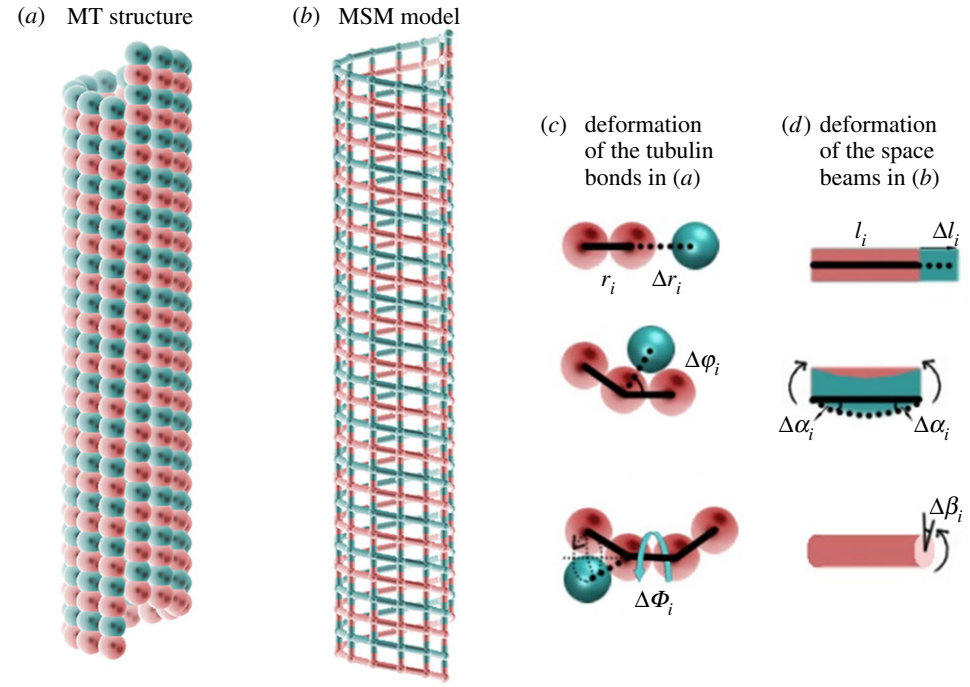

Figure 1. (*a*) Structural representation of an MT with tubulin interactions; (*b*) the MSM model developed for the MT with elastic beams characterizing the tubulin interactions; (*c*) the deformation patterns of the tubulin bonds of the MT; and (*d*) the space beams of the MSM model. (Online version in colour.)

of MT structure and stiffness in pathological and physiological processes. Thus, the distance $r = 0.1$ m is selected here between the dipole and MTs to demonstrate such a design of the MT-based biosensor. In the meantime, it is understood that the amplitude of time-dependent EF should be large enough to excite the forced vibration of MTs with sufficiently large amplitude and thus easy to identify by, for example, vibration energy absorption. Safety is another issue that needs to be taken into consideration. $|\boldsymbol{E}| = 20\,\mathrm{V\,m^{-1}}$ was selected here as it is relatively strong but safe for humans according to World Health Organization and Federal Office for Radiation Safety, Germany [32]. In addition, the fixed–fixed end conditions were imposed on the 13–3 MT in figure 2. The vibrations of the MT are stimulated by the alternating EF via the corresponding electrical force $\boldsymbol{F} = \boldsymbol{E}q$ on MT tubulins. In this study, the vibration analysis was carried out based on the MSM model [18] developed for 13–3 MTs as shown above. The details of the mathematical techniques used in vibration analyses are introduced in the electronic supplementary material.

Moreover, a parametric study is conducted for the transverse vibration of MTs in cytosol across a range of damping effects and frequencies up to 50 MHz. The damping force F_d on the MT monomers is used to characterize the energy dissipation in viscous flow of cytosol and calculated based on the slide film damping theory accounting for the damping effect of microfluid between two moving microscale objects [33,34]. First, a non-slip boundary condition associated with a continuous MT–cytosol interface was considered in calculating F_d. After that, damping reduction coefficient P from 0.0001 to 0.1 was introduced to estimate the reduced damping effect, i.e. the damping force on the monomers decreases to $F_\mathrm{Rd} = F_\mathrm{d} \times P$. Meanwhile, the quality factor $Q = \omega_m/\triangle\omega$ was also calculated for the damped MT vibration, where ω_m is the resonant frequency, A_m is the amplitude of the resonance peak for damped vibration and $\triangle\omega$ is the frequency increment at the points with amplitude $A_m/\sqrt{2}$ [35,36]. The details of the theory and the damped model used in this work are shown in the electronic supplementary material. Here, it should be pointed out that these calculations provide insights into how much reduction is required to achieve prominent MT vibration in cells. The possible reduction of cytosol damping may originate from the relative sliding [14] and/or the van der Waals interaction between MT and cytosol, i.e. a non-continuous MT–cytosol interface. Other factors may also exert an influence on the damping of cytosol. For example, in [37] the wettability and especially the slip length are identified as major factors affecting water damping effect on the longitudinal vibration of polarized nanorods. However, the reduction of cytosol damping due to these factors has not been examined systematically for all the possible vibration modes based on experiments or atomistic simulations.

3. Results and discussions

In this section, the forced vibrations of MTs subject to an alternating EF were explored, and the influence of the abnormal interaction between adjacent tubulins was examined. In addition, a parametric study was also conducted to evaluate the influence of the reduced cytosol damping due to the distinctive MT–cytosol interface at the nanoscale.

3.1. Electromechanical vibrations

3.1.1. Vibrations excited by transverse electric field

As mentioned in §1, the investigations on the free vibration of MTs have achieved multiple progresses [10,11,38]. The eigenvalue vibration analysis was efficiently used to predict the vibration modes and resonant frequencies of MTs [10,13,20]. The associated vibration amplitude, however, cannot be obtained by solving the eigenvalue problems. In this study, we further studied the forced vibrations of MTs

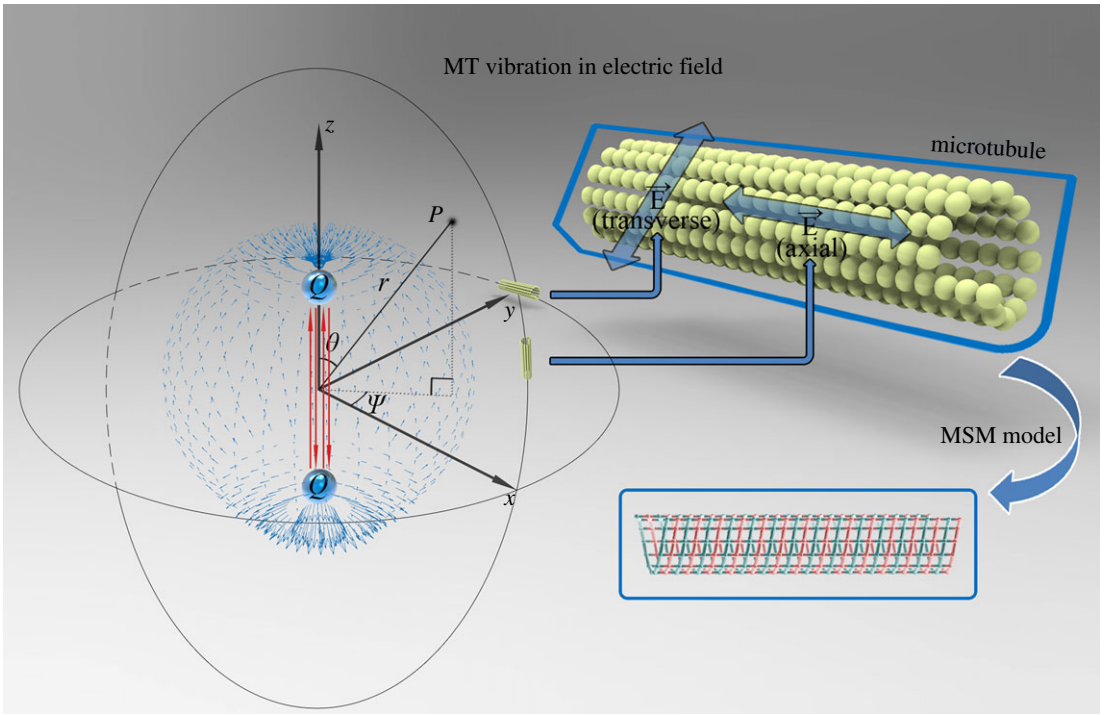

Figure 2. EF generated by a Hertzian dipole in a spherical polar coordinate system and its vector directions at the locations where the MT was placed. (Online version in colour.)

excited by a uniform EF. The major concerns are (i) the possible vibration modes and associated frequencies that can be excited by an alternating EF in the transverse or axial direction of MTs and (ii) 'vibration amplitude–EF frequency' relations, which are crucial in predicting the equivalent dipole moment of vibrating MTs [6] and facilitating the design of MT-based biosensors based on the electromechanical vibration of MTs [14].

First, the forced vibrations of MTs excited by the transverse alternating EF (figure 2) are presented in figure 3 in comparison with the free vibrations obtained for the same MT via the eigenvalue analysis. Figure 3*a* shows seven transverse free vibrations whose resonant frequency upshifts with the growing half wavenumber and falls in the range of (0 MHz, 250 MHz). The amplitudes of the MT are measured at the three points whose distance from the left MT end is $L/2$, $L/4$ and $L/8$, respectively (L is the MT length; figure 3*a*). In the obtained amplitude–frequency spectra (figure 3*b*), seven peaks were picked up in the vicinity of the resonant frequencies. Accordingly, seven forced transverse modes were achieved, which are identical to the seven free vibration modes shown in figure 3. Meanwhile, for a given amplitude the widths of frequency range (W_{fr}) of the peaks (the frequency span around the frequency peak with the amplitude greater than the given value) associated with the odd half wavenumbers 1, 3, 5 and 7 are found to be greater than those corresponding to the even half wavenumbers 2, 4 and 6. In addition, among the peaks with an odd half wavenumber, the W_{fr} increases with decreasing wavenumber or declining frequency. The observation suggested that the excitations of the MT vibration with relatively large odd half wavenumber and particularly even half wavenumbers are very sensitive to the selected frequency of the EF, and accordingly, showed narrow or sharp peaks in the amplitude–frequency spectra. They can be obtained only if the frequency of excitation is the same as the corresponding resonant frequency of MTs. A small deviation from the resonant frequency would extinguish these even modes. It follows that the odd transverse modes of MTs with low frequency can be excited in a wider range of frequency, and thus are promising for their applications in MT-based biosensors.

3.1.2. Vibrations stimulated by axial electric field

Possible vibration behaviours of MTs other than transverse modes have been predicted by eigenvalue analysis [6,10]. Such vibration modes can also be achieved by applying an alternating EF in the axial direction (figure 4*a*). Figure 4*b–d* shows the three typical examples and the associated amplitude–frequency spectra. The radial breathing mode (RBM) with a circular cross section and the axial half wavenumber $m = 1$ was observed at around 53.019 MHz (figure 4*b*). In RBM, the α and β tubulins of the MT oscillate in the radial direction as if the MT was breathing with a time-dependent radius. The vibrational radial displacement is distributed uniformly along the perimeter of MT cross section. Along the MT length, the distribution however becomes non-uniform and characterized by the axial half wavenumber m, which increases with rising frequency. For instance, the frequency 159.291 MHz of the RBM with $m = 3$ is three times as much as the 53.019 MHz associated with $m = 1$. In addition, the circumferential modes with a non-circular cross section [11,39] were also found in figure 4*c* at around 585.639 MHz. The radial amplitudes (figure 4*a*) at the middle point of the MTs were recorded in the amplitude–frequency spectra for the vibration modes (figure 4*b*,*c*). Here, two peaks are observed around the resonance frequencies (of RBMs) 53.019 MHz (figure 4*b*) and 585.639 MHz (figure 4*c*), respectively. The amplitude is of the order of 0.02 nm at 53.019 $\pm$ 0.001 MHz and 0.0003 nm at 585.639 $\pm$ 0.001 MHz, which is two orders of magnitude smaller than the first one. Meanwhile, in figure 4*c* another peak of circumferential mode

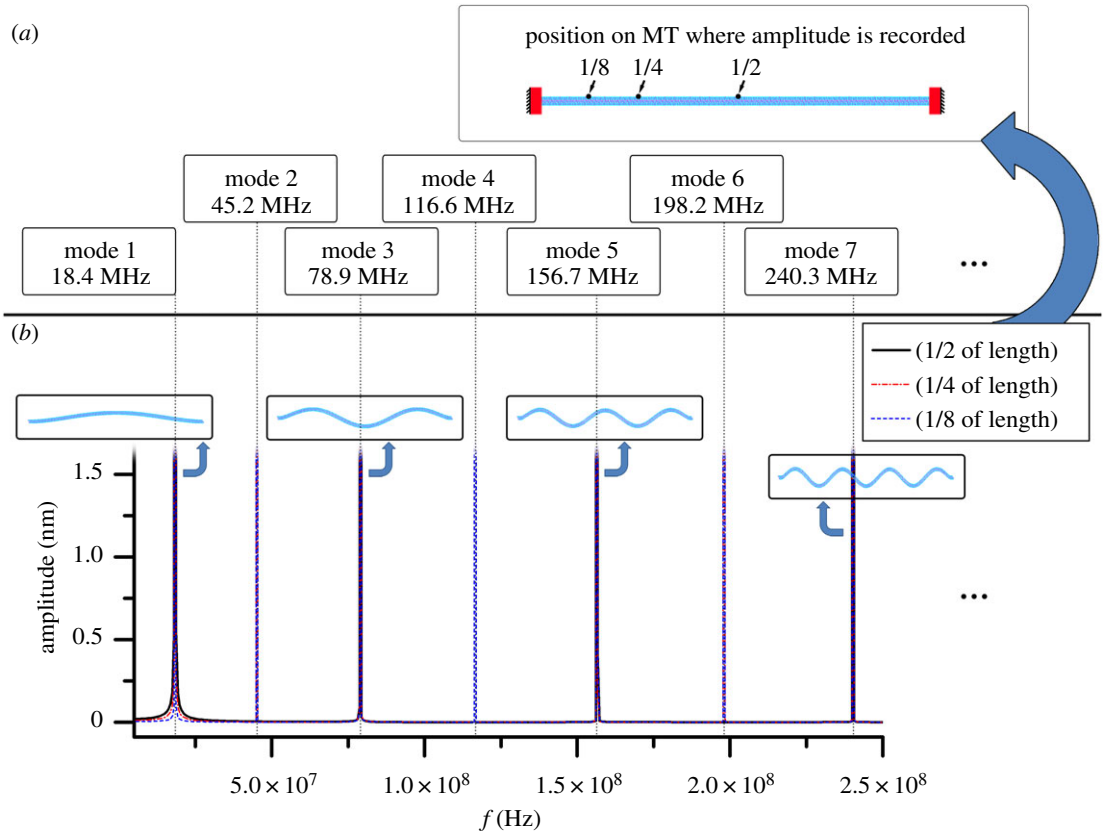

Figure 3. The comparison between the eigenvalue transverse vibration modes and the vibrations of MTs excited by the EF in the transverse direction. (*a*) Transverse modes in eigenvalue analysis and (*b*) forced vibration under harmonic EF. (Online version in colour.)

was also observed at a frequency slightly lower than 585.639 MHz of RBM.

In addition to RBMs, the axial vibration mode at around 377.840 MHz possesses the highest amplitude as shown in figure 4*d*. Specifically, a sinusoidal alternating EF with an amplitude of 20 V m^{-1} can excite the axial vibration of individual MTs with a W_{fr} (associated with amplitude greater than 0.1 nm) around 150 kHz, i.e. from 377.915 MHz to 377.765 MHz. In this study, the amplitude 0.1 nm is selected as a reference oscillatory displacement. The W_{fr} of a resonant peak is then defined as the frequency range (around the peak) associated with the amplitude greater than 0.1 nm. This definition allows us to compare the W_{fr} between different resonant peaks.

3.2. Dependence of vibration on tubulin interaction

It was shown recently [40] that cell stiffness can be used as a biomarker to identify cancerous cells among surrounding healthy cells. Herein, MTs are known as one of the major structural elements responsible for cell stiffness and the variation of MT stiffness can be reflected by the frequency shift of MT vibration excited by an EF [14]. It is thus expected that MT frequency can be used as a bio-indicator to quantify the changes in the structural stiffness of MTs in diseased cells.

It is understood that the structural domains of tubulins, i.e. the N-terminal, intermediate and C-terminal domains [41], may contribute to heterodimer stability, longitudinal and lateral PF interactions, nucleotide exchange and hydrolysis, and MT–protein interactions [41]. Disease-causing amino acid substitutions are found among the three domains of tubulins and therefore predicted to perturb a range of MT functions [42]. Specifically, the disease-causing substitutions in TUBB2B alter amino acids in domains important for GTP binding, heterodimer stability and longitudinal interactions, and those in TUBB3 are located primarily in regions that regulate GTP binding, heterodimer stability, and longitudinal and lateral interactions. It follows that the variation of MT stiffness may arise from the abnormal interactions between adjacent tubulins due to pathological changes (e.g. the above-mentioned disease-causing substitutions or the cancer progression induced structural remodelling of MTs) in the human body [23]. It is thus of great interest to study the dependence of the elastic moduli and vibration frequency of MTs on the strength of tubulin interaction. The outcomes have potential applications in developing biosensors for the biophysical properties of individual MTs or cells.

To mimic this scenario, we have adjusted the strength of longitudinal and helical tubulin interactions by varying the values of the force constants k_i^r, k_i^φ, and k_i^τ (§2.1) that control changes in the bond length, the bond angle and the dihedral angle of tubulin interactions (figure 1*c*,*d*). k_i^r, k_i^φ and k_i^τ for normal cells were obtained in [21,23] and replaced in this study by Ωk_i^r, Ωk_i^φ and Ωk_i^τ where Ω is a coefficient ranging from 0.2 to 2, which allows us to produce the elastic modulus close to the experimentally obtained stiffness of cancer cells at different progression stages [40]. First, Young's modulus Y and shear modulus G are measured for the MTs where the strength of the tubulin interactions varies by an order of magnitude. The method used here to measure the elastic moduli is demonstrated in [18]. Subsequently, the fundamental vibration is studied for the above MTs subject to a transverse EF. The aim of this study is to establish the correlation between the tubulin interaction and the W_{fr} at the resonant frequency, which is defined by the frequency span with an amplitude greater than 0.1 nm [6].

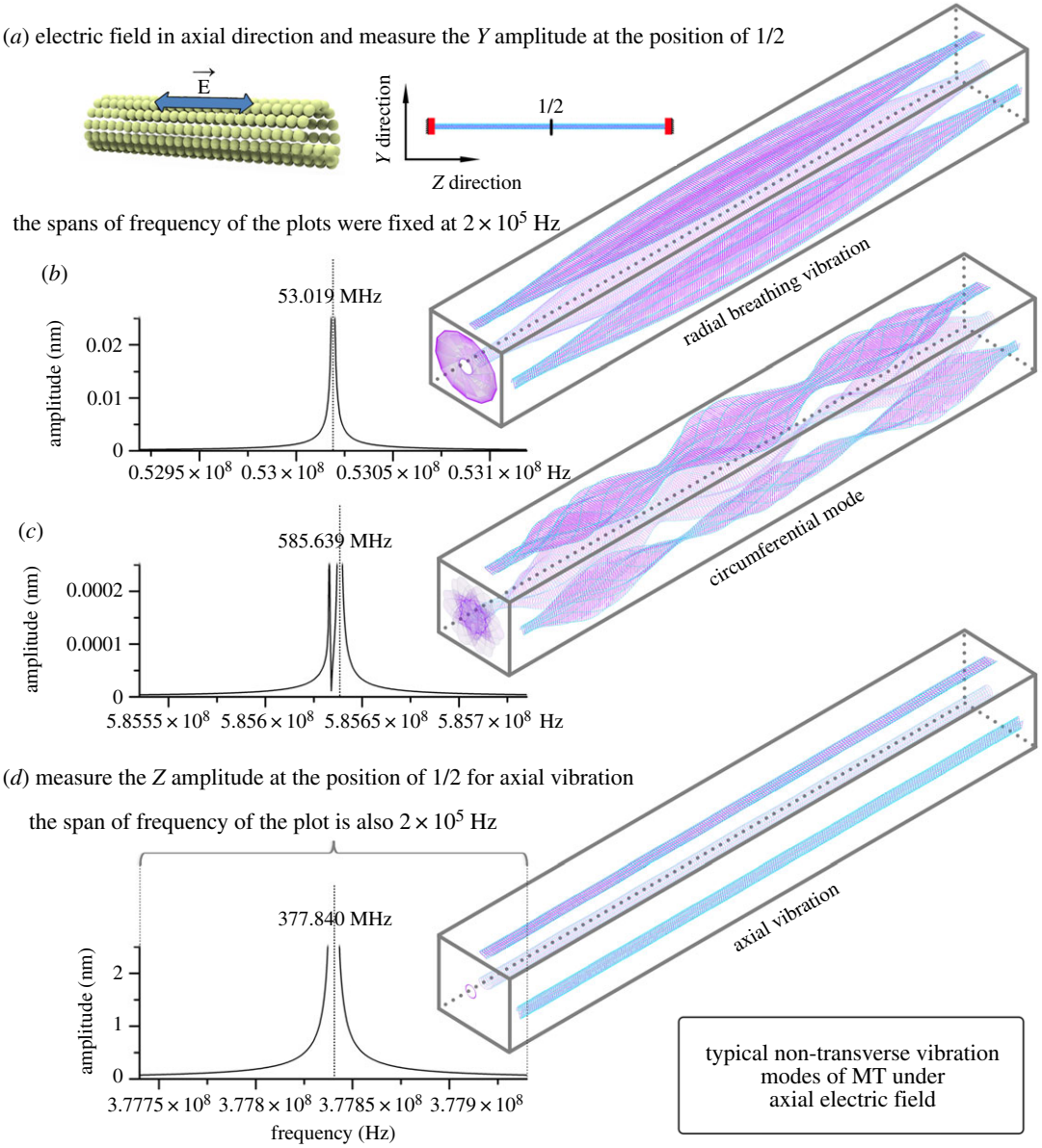

Figure 4. The vibration modes of MTs excited by the EF in the axial direction. (Online version in colour.)

As shown in figure 5*a*, when the longitudinal interaction is altered with Ω rising from 0.2 to 2, G changes slightly around 1.5 MPa [43], while Y increases linearly from 0.17 to 1.71 GPa by a factor of 10.06. In the same process, the fundamental frequency rises from 9.02 to 23.67 MHz (by a factor of 2.62) while the W_{fr} decreases from 7.05 to 2.48 MHz (by 65%). The trend of the properties and dynamic responses to change with helical interaction is plotted in figure 5*b*. In contrast to the longitudinal interaction effect, Y remains nearly unchanged while G grows linearly from 0.32 to 2.86 MPa by a factor of 8.94 with rising Ω. It also is noted in figure 5*b* that when Ω rises from 0.2 to 2, the fundamental frequency rises from 13.67 MHz to 19.41 MHz (by 42%) while the W_{fr} decreases from 4.30 to 3.03 MHz (by 30%). The effect of the helical interaction on the frequency and the W_{fr} is found to be smaller than the effect of the longitudinal interaction.

Herein, the longitudinal interaction is found to be important for axial Young's modulus, while the helical interaction is mainly responsible for shear modulus. These results are in agreement with [23,44]. Consistent with this observation, the longitudinal interaction also plays a major role in fundamental (transverse) vibration, where axial Young's modulus has a predominant effect over shear modulus. Moreover, the fundamental frequency also changes with the variation of the helical interaction and is found to be more sensitive to the helical interaction weakening than its strengthening. For instance, when Ω falls from 1 to 0.2, i.e. the helical interaction is weakened by 80%, the fundamental frequency decreases by 26% while it only increases by 5% when Ω rises from 1 to 2, i.e. the helical interaction is strengthened by 100%.

The above study indeed shows a typical example that the nanostructures of subcellular components like MTs may have a substantial influence on their overall static and dynamic responses [1]. The prominent role of longitudinal interaction in the transverse MT vibration originates from its influence on axial Young's modulus that controls the bending or transverse deformation of MTs. In the meantime, the helical interaction is responsible for the resistance of MTs to shear deformation or inter-PF sliding. Weakening the helical interaction leads to significant inter-PF sliding [19,23,45], which however is prohibited when the interaction is strengthened. This explains the relatively large frequency shift due to the helical interaction weakening. These results obtained in the present simulations show the potential of polarized MTs as a biosensor and frequency as a possible

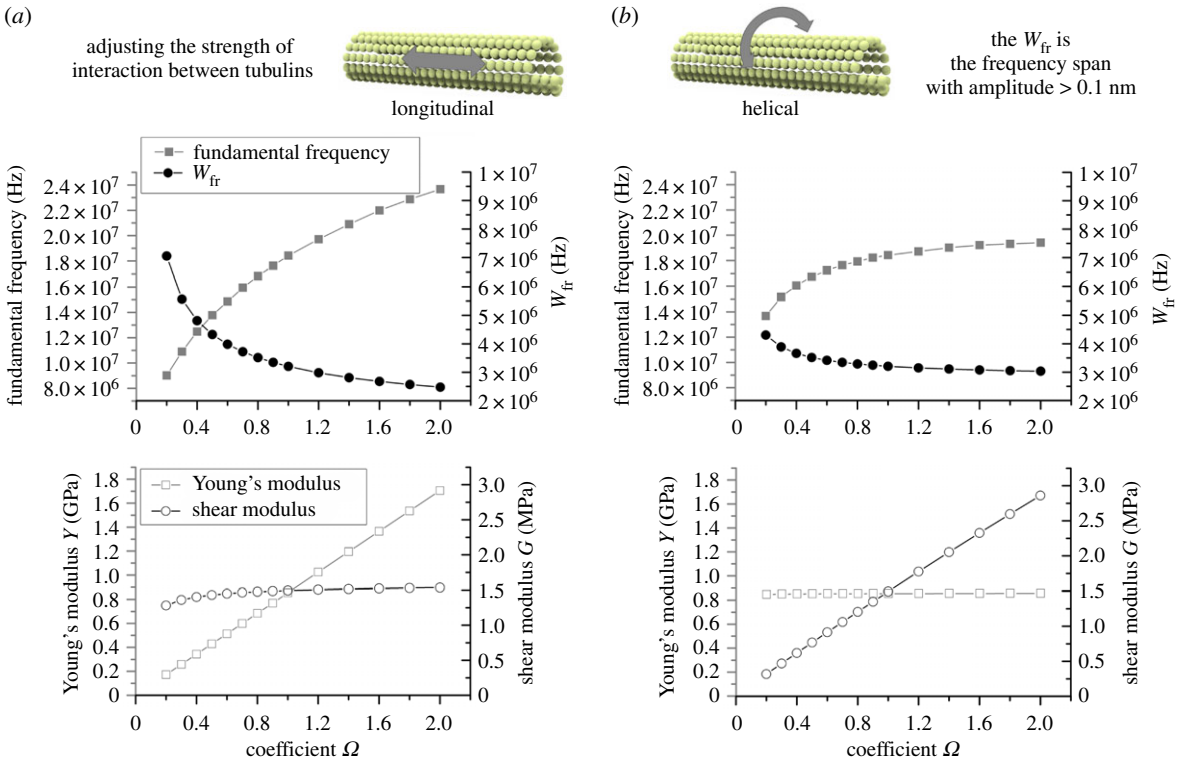

Figure 5. The changes in vibrational responses and elastic moduli of MTs as a result of (*a*) abnormal longitudinal interactions between tubulins and (*b*) abnormal helical interactions between tubulins. (Online version in colour.)

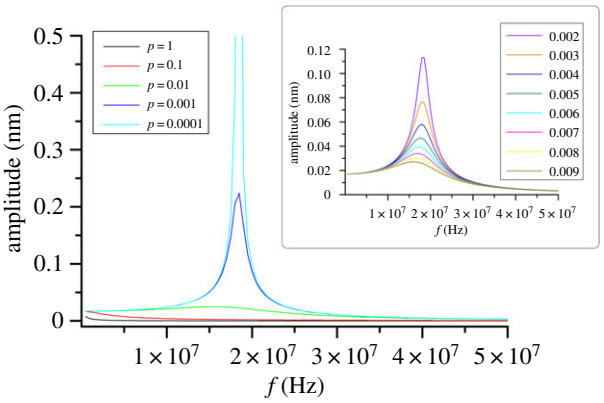

Figure 6. The changes in responses of damped MT vibration in cytosol due to different damping reduction factors. (Online version in colour.)

biomarker in detecting the property and structural changes in individual MTs or cells in physiological or pathological processes.

3.3. Evaluation of reduced cytosol damping

In previous sections, the EF-excited vibrations of individual MTs are investigated without considering any damping effect in the intracellular environment. In reality, MTs are submerged in cytosol of cells (70% water). Thus, cytosol damping cannot be avoided. On the other hand, the damping effect may reduce to some extent due to, for example, the possible MT–cytosol sliding and the van der Waals interaction although we are still waiting for experiments or simulations to confirm this assumption. Therefore, it is of interest to conduct a parametric study of cytosol damping and find the condition under which the prominent vibration of MTs can be excited by EF. It was shown in §2 that a coefficient P was introduced to decrease the frictional forces on the MT due to surrounding cytosol and thus measure the reduction of the damping effect. The amplitude–frequency spectra are calculated in figure 6 for the transverse vibrations with P rising from 0.0001 to 1. For the continuous MT–cytosol interface with $P = 1$, viscous damping is so strong that it can extinguish the vibrations of MTs, which is found to be in agreement with [46]. When the damping effect decreases to $P = 0.1$, the amplitude increases but is still very small. Further decreasing P to 0.01, 0.001 and to 0.0001 leads to the increasing amplitude of the order of 0.02 nm, 0.2 nm and 1.2 nm, respectively. Thus, transverse vibration with amplitude greater than 0.1 nm [6] can be achieved when the cytosol damping effect can decrease by three orders of magnitude due to the unique features of the MT–cytosol interface at the nanoscale. To reveal the trend of quality factor Q in this process, we have calculated the frequency spectra with P ranging from 0.002 to 0.009 in the inset of figure 6. In the figure, Q is found to increase with decreasing damping effect measured by P and at $P < 0.003$, $Q > 4.3$ can be obtained. Here, it is worth mentioning that decreasing cytosol damping leads to greater Q mainly by raising the amplitude. In this process, the W_{fr} also grows with increasing Q or decreasing P.

Here, it should be noted that the present study evaluates the reduction of cytosol damping required to stimulate prominent vibration of MTs in cells. It is however not clear whether the unique MT–cytosol interface can finally achieve the goal. In addition, the experimental evidence of MT vibration in cells is still not available in the literature. There are two possibilities. (i) The MT–cytosol interface cannot substantially decrease the damping effect of cytosol which finally quenches the vibrations of MTs in cells. (ii) More advanced signal acquisition technique is required to identify the resonance of nanoscale components of cells and tissues. Indeed,

these issues as well as many other technical challenges need to be addressed before one can eventually realize the proposed MT-based biosensors.

4. Conclusion

In the present paper, an alternating EF was used to excite the forced vibration of polarized MTs in different modes. The possibility was also examined to detect the abnormal tubulin interaction in pathological processes by measuring the changes in the frequency and elastic moduli of MTs. The effect of cytosol damping is also evaluated for the transverse vibration of the MT.

It is found that a transverse EF is able to excite transverse vibrations of MTs where frequency upshifts from 18.4 to 240.3 MHz when the half axial wavenumber rises from one to seven. The vibrations with the even half wavenumbers are hard to excite as they show a very narrow W_{fr} on the vibration spectra, while it is relatively easy to achieve those with odd half wavenumber due to their much wider W_{fr} which increases with the decreasing frequency.

An axial EF is found to generate RBMs (with a circular cross section) of MTs, which can be observed in the vibration spectra at a frequency around 53.019 MHz and 159.291 MHz, much higher than the frequencies of the transverse vibrations with the same half axial wavenumber. The circumferential vibrations with non-circular cross section are also achieved at 585.639 MHz. In addition, the axial vibration of frequency 377.840 MHz can also be excited, where the amplitude is found to be greater than other modes stimulated by an axial EF.

For MTs in cells, the excitation of prominent vibrations depends largely on the possible MT–cytosol sliding at the interface, which may substantially reduce cytosol damping. The transverse vibration with an amplitude greater than 0.1 nm and quality factor Q larger than 4.3 can be achieved by applying an EF of 20 V m^{-1} provided that the sliding MT–cytosol interface can largely decrease the damping by three orders of magnitude relative to the cytosol damping due to a normal continuous MT–cytosol interface.

In addition, it is also found that the longitudinal tubulin interaction determines the axial Young's modulus that controls the bending deformation or the transverse vibration, while the helical tubulin interaction mainly decides shear modulus and the inter-PF sliding. Thus, changes in the longitudinal or helical interaction in pathological processes can be detected via the variation of elastic moduli and the shift of MT frequency as promising biomarkers.

Indeed, correlating the pathological changes of MTs to their responses to an alternating EF is crucial for the development of MT-based biosensors. Hence, the dependence of MT frequency on the tubulin interaction achieved here not only reveals the structure–property relation of MTs, but also provides useful guidance to the development of MT-based biosensors to detect the changes in the mechanical properties and structure of individual MTs or cells.

Data accessibility. The method and theory for the simulations are provided in the paper and the electronic supplementary material. The primary data (codes) are also provided in the electronic supplementary material.

Authors' contributions. S.L. carried out the simulations and analysis, participated in the design of the study and drafted the manuscript; C.W. participated in the design of the study and helped draft the manuscript; P.N. helped draft the manuscript. All authors gave final approval for publication and agree to be held accountable for the work performed therein.

Competing interests. We have no competing interests.

Funding. S.L. acknowledges the financial support from the China Scholarship Council (CSC) and College of Engineering, Swansea University.

References

1. Howard J, Hyman AA. 2003 Dynamics and mechanics of the microtubule plus end. *Nature* **422**, 753–758. (doi:10.1038/nature01600)
2. Barzanjeh S, Salari V, Tuszynski J, Cifra M, Simon C. 2017 Optomechanical proposal for monitoring microtubule mechanical vibrations. *Phys. Rev. E* **96**, 012404. (doi:10.1103/PhysRevE.96.012404)
3. Stracke R, Böhm K, Wollweber L, Tuszynski J, Unger E. 2002 Analysis of the migration behaviour of single microtubules in electric fields. *Biochem. Biophys. Res. Commun.* **293**, 602–609. (doi:10.1016/S0006-291X(02)00251-6)
4. Nogales E, Wolf SG, Downing KH. 1998 Structure of the $\alpha\beta$ tubulin dimer by electron crystallography. *Nature* **391**, 199–203. (doi:10.1038/30288)
5. Pizzi R, Strini G, Fiorentini S, Pappalardo V, Pregnolato M. 2011 Evidences of new biophysical properties of microtubules. In *Artificial neural networks engineering: tools, techniques and tables* (ed. SJ Kwon). Mathematics Research Developments Series. New York, NY: Nova Science Publishers.
6. Cifra M, Pokorný J, Havelka D, Kučera O. 2010 Electric field generated by axial longitudinal vibration modes of microtubule. *Biosystems* **100**, 122–131. (doi:10.1016/j.biosystems.2010.02.007)
7. Sirenko YM, Stroscio MA, Kim K. 1996 Elastic vibrations of microtubules in a fluid. *Phys. Rev. E* **53**, 1003–1010. (doi:10.1103/PhysRevE.53.1003)
8. Pokorný, J. 2003 Viscous effects on polar vibrations in microtubules. *Electromagn. Biol. Med.* **22**, 15–29. (doi:10.1081/JBC-120020349)
9. Kasas S, Cibert C, Kis A, Rios PL, Riederer B, Forro L, Dietler G, Catsicas S. 2004 Oscillation modes of microtubules. *Biol. Cell* **96**, 697–700. (doi:10.1016/j.biolcel.2004.09.002)
10. Wang CY, Ru CQ, Mioduchowski A. 2006 Vibration of microtubules as orthotropic elastic shells. *Physica E* **35**, 48–56. (doi:10.1016/j.physe.2006.05.008)
11. Wang CY, Zhang LC. 2008 Circumferential vibration of microtubules with long axial wavelength. *J. Biomech.* **41**, 1892–1896. (doi:10.1016/j.jbiomech.2008.03.029)
12. Arani AG, Abdollahian M, Jalaei M. 2015 Vibration of bioliquid-filled microtubules embedded in cytoplasm including surface effects using modified couple stress theory. *J. Theor. Biol.* **367**, 29–38. (doi:10.1016/j.jtbi.2014.11.019)
13. Li S, Wang CY, Nithiarasu P. 2017 Three-dimensional transverse vibration of microtubules. *J. Appl. Phys.* **121**, 234301. (doi:10.1063/1.4986630)
14. Pokorný, J., Vedruccio C, Cifra M, Kučera O. 2011 Cancer physics: diagnostics based on damped cellular elastoelectrical vibrations in microtubules. *Eur. Biophys. J.* **40**, 747–759. (doi:10.1007/s00249-011-0688-1)
15. Deriu MA, Enemark S, Soncini M, Montevecchi FM, Redaelli A. 2007 Tubulin: from atomistic structure to supramolecular mechanical properties. *J. Mater. Sci.* **42**, 8864–8872. (doi:10.1007/s10853-007-1784-6)
16. Enemark S, Deriu MA, Soncini M, Redaelli A. 2008 Mechanical model of the tubulin dimer based on molecular dynamics simulations. *J. Biomech. Eng.* **130**, 041008. (doi:10.1115/1.2913330)
17. Deriu MA, Soncini M, Orsi M, Patel M, Essex JW, Montevecchi FM, Redaelli A. 2010 Anisotropic elastic network modeling of entire microtubules. *Biophys. J.* **99**, 2190–2199. (doi:10.1016/j.bpj.2010.06.070)
18. Zhang J, Wang CY. 2014 Molecular structural mechanics model for the mechanical properties of

microtubules. *Biomech. Model. Mechanobiol.* **13**, 1175–1184. (doi:10.1007/s10237-014-0564-x)

19. Chrétien D, Fuller SD. 2000 Microtubules switch occasionally into unfavorable configurations during elongation. *J. Mol. Biol.* **298**, 663–676. (doi:10.1006/jmbi.2000.3696)
20. Zhang J, Wang CY. 2016 Free vibration analysis of microtubules based on the molecular mechanics and continuum beam theory. *Biomech. Model. Mechanobiol.* **15**, 1069–1078. (doi:10.1007/s10237-015-0744-3)
21. Ji XY, Feng XQ. 2011 Coarse-grained mechanochemical model for simulating the dynamic behavior of microtubules. *Phys. Rev. E* **84**, 031933. (doi:10.1103/PhysRevE.84.031933)
22. Zhang J, Meguid S. 2014 Buckling of microtubules: an insight by molecular and continuum mechanics. *Appl. Phys. Lett.* **105**, 173704. (doi:10.1063/1.4900943)
23. Li S, Wang C, Nithiarasu P. 2018 Structure–property relation and relevance of beam theories for microtubules: a coupled molecular and continuum mechanics study. *Biomech. Model. Mechanobiol.* **17**, 339–349. (doi:10.1007/s10237-017-0964-9)
24. Vater W, Stracke R, Boehm K, Speicher C, Weber P, Unger E. 1998 Behaviour of individual microtubules and microtubule bundles in electric fields. In *6th Foresight Conf. on Molecular Nanotechnology, Santa Clara, CA, USA, 12–15 November 1998*.
25. Vassilev PM, Dronzine RT, Vassileva MP, Georgiev GA. 1982 Parallel arrays of microtubles formed in electric and magnetic fields. *Biosci. Rep.* **2**, 1025–1029. (doi:10.1007/BF01122171)
26. Vassilev P, Kanazirska M. 1985 The role of cytoskeleton in the mechanisms of electric field effects and information transfer in cellular systems. *Med. Hypotheses* **16**, 93–96. (doi:10.1016/0306-9877(85)90065-9)
27. Brown JAM. 2000 A study of the interactions between electromagnetic fields and microtubules: ferroelectric effects, signal transduction and electronic conduction. PhD thesis, University of Alberta, Edmonton, Canada.
28. Mershin A, Kolomenski AA, Schuessler HA, Nanopoulos DV. 2004 Tubulin dipole moment, dielectric constant and quantum behavior: computer simulations, experimental results and suggestions. *Biosystems* **77**, 73–85. (doi:10.1016/j.biosystems.2004.04.003)
29. Grant IS, Phillips WR. 2013 *Electromagnetism*. Chichester, UK: John Wiley & Sons.
30. Zahn M. 1979 *Electromagnetic field theory: a problem solving approach*. New York, NY: John Wiley & Sons.
31. Griffiths DJ. 1999 *Introduction to electrodynamics*. Upper Saddle River, NJ: Prentice Hall.
32. WHO. Electromagnetic fields (EMF). See http://www.who.int/peh-emf/about/WhatisEMF/en/index3.html
33. Chang H, Zhang Y, Xie J, Zhou Z, Yuan W. 2010 Integrated behavior simulation and verification for a MEMS vibratory gyroscope using parametric model order reduction. *J. Microelectromech. Syst.* **19**, 282–293. (doi:10.1109/JMEMS.2009.2038284)
34. Cho Y-H, Kwak BM, Pisano AP, Howe RT. 1994 Slide film damping in laterally driven microstructures. *Sens. Actuators, A* **40**, 31–39. (doi:10.1016/0924-4247(94)85027-5)
35. Liu X, Civet Y, Perriard Y. 2015 Quality factor and vibration amplitude estimation of a piezoelectric-actuated system using impedance measurements. In *18th Int. Conf. on Electrical Machines and Systems (ICEMS), Pattaya, Thailand, 25–28 October 2015*, pp. 1993–1996. (doi:10.1109/ICEMS.2015.7385367)
36. Piersol AG, Harris CM. 2017 *Harri's shock and vibration handbook*, 5th edn. New York, NY: McGraw-Hill.
37. Krivosudský, O, Cifra M. 2016 Microwave absorption by nanoresonator vibrations tuned with surface modification. *Europhys. Lett.* **115**, 44003. (doi:10.1209/0295-5075/115/44003)
38. Wang CY, Zhang J, Fei YQ, Murmu T. 2012 Circumferential nonlocal effect on vibrating nanotubules. *Int. J. Mech. Sci.* **58**, 86–90. (doi:10.1016/j.ijmecsci.2012.03.009)
39. Wang C, Ru C, Mioduchowski A. 2005 Free vibration of multiwall carbon nanotubes. *J. Appl. Phys.* **97**, 114323. (doi:10.1063/1.1898445)
40. Luo Q, Kuang D, Zhang B, Song G. 2016 Cell stiffness determined by atomic force microscopy and its correlation with cell motility. *Biochim. Biophys. Acta* **1860**, 1953–1960. (doi:10.1016/j.bbagen.2016.06.010)
41. Löwe J, Li H, Downing K, Nogales E. 2001 Refined structure of $\alpha\beta$-tubulin at 3.5 Å resolution. *J. Mol. Biol.* **313**, 1045–1057. (doi:10.1006/jmbi.2001.5077)
42. Tischfield MA, Cederquist GY, Gupta ML, Engle EC. 2011 Phenotypic spectrum of the tubulin-related disorders and functional implications of disease-causing mutations. *Curr. Opin. Genet. Dev.* **21**, 286–294. (doi:10.1016/j.gde.2011.01.003)
43. Kis A, Kasas S, Babić B, Kulik A, Benoit W, Briggs G, Schönenberger C, Catsicas S, Forro L. 2002 Nanomechanics of microtubules. *Phys. Rev. Lett.* **89**, 248101. (doi:10.1103/PhysRevLett.89.248101)
44. Pampaloni F, Lattanzi G, Jonas A, Surrey T, Frey E, Florin EL. 2006 Thermal fluctuations of grafted microtubules provide evidence of a length-dependent persistence length. *Proc. Natl Acad. Sci. USA* **103**, 10 248–10 253. (doi:10.1073/pnas.0603931103)
45. Chrétien D, Flyvbjerg H, Fuller SD. 1998 Limited flexibility of the inter-protofilament bonds in microtubules assembled from pure tubulin. *Eur. Biophys. J.* **27**, 490–500. (doi:10.1007/s002490050159)
46. Foster KR, Baish JW. 2000 Viscous damping of vibrations in microtubules. *J. Biol. Phys.* **26**, 255–260. (doi:10.1023/A:1010306216654)